Geomechanics and Engineering, *Vol. 23, No. 3 (2020) 289-300*
DOI: https://doi.org/10.12989/gae.2020.23.3.289

Strain-based stability analysis of locally loaded slopes under variable conditions

Jia-Chen Wang[1a], Hong-Hu Zhu*[1,2], Bin Shi[1b] and Ankit Garg[3,4c]

[1]School of Earth Sciences and Engineering, Nanjing University, Nanjing 210023, China
[2]Key Laboratory of Mountain Hazards and Earth Surface Processes, Chinese Academy of Sciences, Chengdu 610041, China
[3]Department of Civil and Environmental Engineering, Shantou University, Shantou 515063, China
[4]Guangdong Engineering Center for Structure Safety and Health Monitoring, Shantou University, Shantou 515063, China

(Received June 18, 2019, Revised October 9, 2020, Accepted October 26, 2020)

Abstract. With the rapid development of the distributed strain sensing (DSS) technology, the strain becomes an alternative monitoring parameter to analyze slope stability conditions. Previous studies reveal that the horizontal strain measurements can be used to evaluate the deformation pattern and failure mechanism of soil slopes, but they fail to consider various influential factors. Regarding the horizontal strain as a key parameter, this study aims to investigate the stability condition of a locally loaded slope by adopting the variable-controlling method and conducting a strength reduction finite element analysis. The strain distributions and factors of safety in different conditions, such as slope ratio, soil strength parameters and loading locations, are investigated. The results demonstrate that the soil strain distribution is closely related to the slope stability condition. As the slope ratio increases, more tensile strains accumulate in the slope mass under surcharge loading. The cohesion and the friction angle of soil have exponential relationships with the strain parameters. They also display close relationships with the factors of safety. With an increasing distance from the slope edge to the loading position, the transition from slope instability to ultimate bearing capacity failure can be illustrated from the strain perspective.

Keywords: soil strain; slope stability; finite element analysis (FEA); strength reduction method (SRM)

1. Introduction

Slope stability has always been a concern of communities in mountainous regions with growing awareness of safety. Nowadays, many physical parameters have been used as indicators of slope instability, such as displacement, strain, and pore water pressure (Angeli *et al.* 2000, Uchimura *et al.* 2010, Florkiewicz and Kubzdela 2013, Severin *et al.* 2014, Su *et al.* 2017, Xing *et al.* 2019, Liu *et al.* 2020). In the engineering practice, slope stability evaluation and early warning of landslide are usually based on the monitoring data of displacement which have been proved to be direct indicators of slope stability condition.

In the research field of multiple wedge slope stability analysis, the method of kinematics displacement is used to predict both the shear surface location and the factor of safety (FS) (McCombie 2009). Meanwhile, the potential slip surface of soil slopes can also be inferred according to the maximum displacement parameters recorded by slope inclinometers (Pei *et al.* 2019). In slope upgrading works, the large deformation areas are considered as the critical zones to be reinforced (Yang *et al.* 2015). However, sometimes slope failure occurs at a small amount of movements or at localized shearing (Zhu *et al.* 2016). In this situation, one can hardly predict slope failures using the displacement measurements.

Fortunately, strain, as one of the small-scale deformation parameters, is found to be much more sensitive than displacement (Zhu *et al.* 2016, Song *et al.* 2017, Li *et al.* 2020). In recent years, with the aid of distributed strain sensing (DSS) cables vertically installed in boreholes, the shearing zones at a landslide site have been successfully detected (Sun *et al.* 2014, Zhang *et al.* 2018). In the study of Zhu *et al.* (2014), the strain measurements at different elevations can be considered as representative symbols for evaluating slope stability conditions under different loading magnitudes. Shear deformation induced by rainfall is predicted by using the monitoring data of shear strain and pore pressure (Sasahara 2017). In general, the strain-based method of slope stability analysis still is immature. It needs to be further studied considering the influence of slope ratios (elevation/distance), cohesion, friction angles, loading positions, etc.

To investigate the stability condition and failure mechanism of slopes, finite element analysis (FEA) has been widely used (Griffiths and Lane 1999, Liu and Chen 2015, Tu *et al.* 2016, Ouch *et al.* 2017). In comparison with the conventional limit equilibrium method (LEM), the main advantage of FEA is that the slope deformation can be calculated. The factors of safety of slopes under various conditions can be obtained by the strength reduction method

*Corresponding author, Professor
E-mail: zhh@nju.edu.cn
[a]Postgraduate Student
E-mail: wang_jc@smail.nju.edu.cn
[b]Professor
E-mail: shibin@nju.edu.cn
[c]Associate Professor
E-mail: ankit@stu.edu.cn

ISSN: 2005-307X (Print), 2092-6219 (Online)

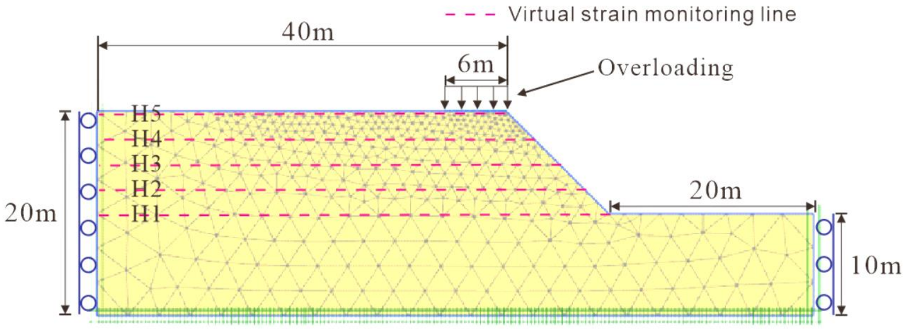

Fig. 1 Numerical model of a soil slope

(SRM), which is found a feasible and effective method in slope stability analysis (Zienkiewicz *et al.* 1975, Cheng *et al.* 2007). The elastic-plastic constitutive models, such as the Mohr-Coulomb model, are generally used to describe the soil behavior.

Besides slope instability, bearing capacity problems of foundations on slopes also pose a potential threat to public safety in hilly areas (Yang *et al.* 2007, Aminpour *et al.* 2017, Sawwaf 2010). In the literature, the discontinuity layout optimization (DLO) method, which involves the use of rigorous mathematical optimization techniques to identify a critical layout of lines of discontinuity forming at failure (Smith and Gilbert 2007), is used to figure out the bearing capacity of slopes (Leshchinsky 2014). Previously, some researchers have applied the FEA and the DLO methods to calculate the ultimate bearing capacity of footings on slopes (Georgiadis 2009, Leshchinsky 2015). It is found that both results agree well with each other.

This study aims to explore an alternative way of analyzing slope stability through the horizontal strain distribution. Numerical simulations have been conducted on locally loaded slopes to investigate the feasibility of strain-based slope stability evaluation considering various factors. The empirical relationships between the strain parameters and the factors of safety are established, which may be used to perform slope stability evaluation based on strain measurements.

2. Numerical model

Two-dimensional finite element analyses on a prototype footing-slope system are performed to identify the deformation trends within the soil slope under different conditions. Using the commercial FEA software Plaxis (Plaxis 2002), a series of numerical models are built. Strain can be considered as a parameter closely related to the slope stress state (Zhu *et al.* 2016). Hence, the horizontal strain is selected to be investigated in this study and five virtual strain monitoring lines are prescribed in the numerical model, as shown in Fig. 1.

The 15-node triangular elements are used to model the slope soil in the simulation. The top width and the clear height of the slope model are 40 m and 10 m, respectively. No horizontal displacement is allowed on the vertical boundaries. Both horizontal and vertical movements are

Table 1 Simulation parameters of the numerical model to be varied

Parameter	Value
Slope ratio (r)	0.25, 0.33, 0.5, 0.67
Cohesion (c)	10 kPa, 12 kPa, 15 kPa, 18 kPa, 20 kPa
Friction angle (φ)	20°, 22°, 25°, 28°, 30°
Loading distance (p)	0 m, 1 m, 2 m, 4 m, 6 m, 8 m, 10 m

Table 2 Unchanged simulation parameters of the numerical model under different conditions

Variable parameters	Constant parameters
Slope ratio (r)	c = 15 kPa, φ = 25°, γ = 20 kN/m^3, p = 0 m, loading pressure = 50 kPa
Cohesion of the soil (c)	r = 1:1, φ = 25°, p = 4 m, γ = 20 kN/m^3, loading pressure = 50 kPa
Friction angle of the soil (φ)	r = 1:1, c = 15 kPa, p = 4 m, γ = 20 kN/m^3, loading pressure = 50 kPa
Loading position (p)	r = 1:1, c = 15 kPa, φ = 25°, γ = 20 kN/m^3, loading pressure = 50 kPa

fixed at the bottom boundary of the numerical model. A distributed load is applied on the slope crest with 6 m width. The loading position and the magnitude are varied to studytheir influence. Meanwhile, the same model is built by using the commercial DLO software LimitState GEO 3.2, which is used to compute the ultimate bearing capacity corresponding to different slope ratios and loading positions. The soil parameters used in this study are the same as those in Zhu *et al.* (2016). According to different simulation situations, the variable-controlling method is used, and the soil strength parameters are adjusted to perform parametric studies. The subsequent section will show the numerical simulation results based on the different parameters listed in Table 1. It should be noticed that the loading position is defined as the distance from the slope edge to the loading (the distance), "p". Other unchanged simulation parameters are listed in Table 2.

3. Results and discussion

According to the previous study of Zhu *et al.* (2016), several strain parameters can be used to evaluate slope

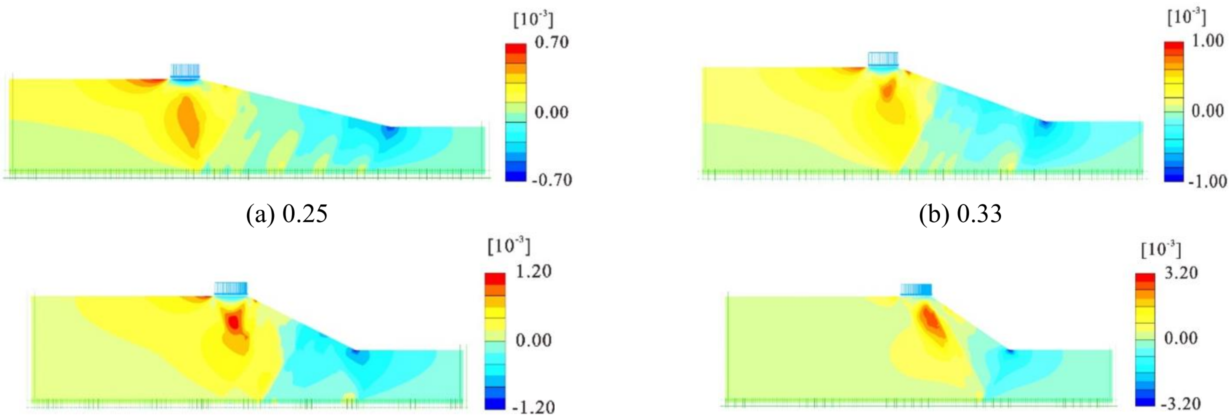

(a) 0.25 (b) 0.33

(c) 0.5 (d) 0.67

Fig. 2 Contour of horizontal strain in slopes with different slope ratios

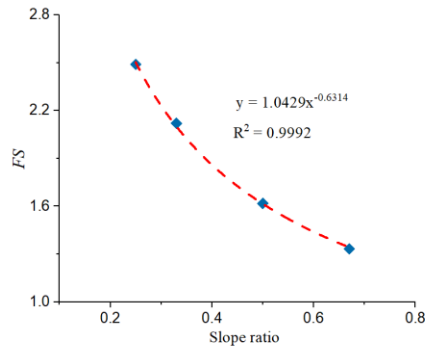

Fig. 3 Relationship between *FS* and slope ratio

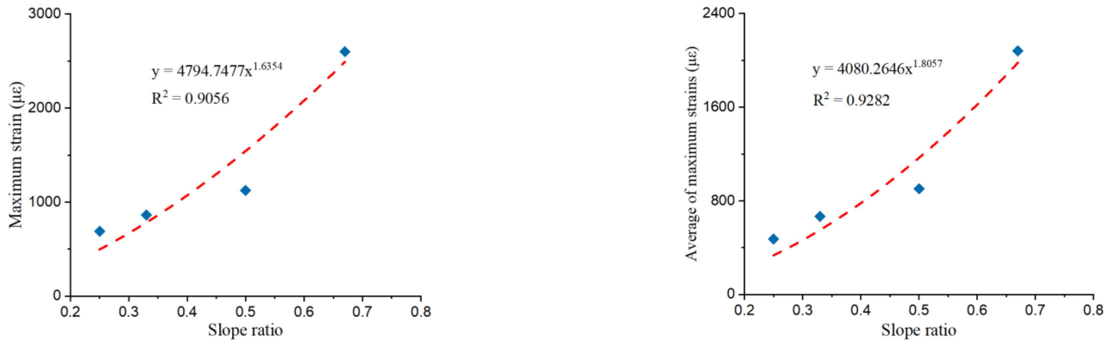

(a) Maximum strain encountered by all the five monitoring lines

(b) Average of maximum strains encountered by all the five monitoring lines

Fig. 4 Relationships between the slope ratio and the strain parameters

stability conditions, especially the maximum strain encountered by all the five monitoring lines ($\varepsilon_{\max}$) and the average of maximum strain encountered by all the five monitoring lines ($\overline{\varepsilon}_{\max}$). In this paper, the characteristics of the two strain parameters and the *FS* in different cases are analyzed.

3.1 Different slope ratios

Figs. 2(a)-2(d) shows the distributions of the horizontal strain correspond to different slope ratios. It can be seen that the distribution of large strain is significantly influenced by slope ratios. Tensile strain can influence the strength of the soil (Duncan *et al.* 2014, Das 2015). With a large slope ratio, the large tensile strain region appears to distribute along the slope surface, especially when the slope ratio is over 0.33. Meanwhile, the larger tensile strain in large ratio slope expands closer to the slope surface, indicating the potential region of the slip surface. The result conforms to the experimental outcome of Zhu *et al.* (2016). For a slope with a relatively low ratio, such as 0.25 and 0.33, the strain concentration region under the loading expands vertically. As for slope stability, Fig. 3 shows the relationship between the slope ratio and the *FS*. The slope with a larger ratio has a lower *FS*, and the relationship between them can be fitted by a high correlation exponential function.

Relationships between the slope ratio and the strain

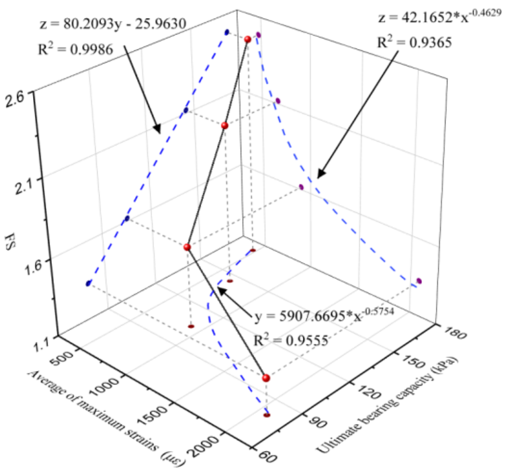

Fig. 5 Relationship among the ultimate bearing capacity, the average of maximum strains encountered by all the five monitoring lines and the *FS*

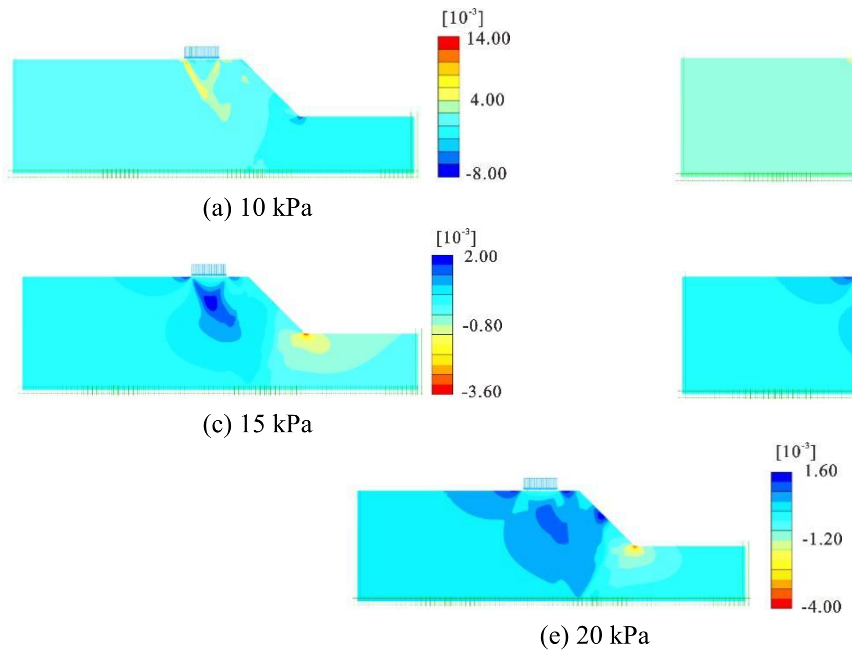

Fig. 6 Contour of horizontal strain in the slope with different values of cohesion

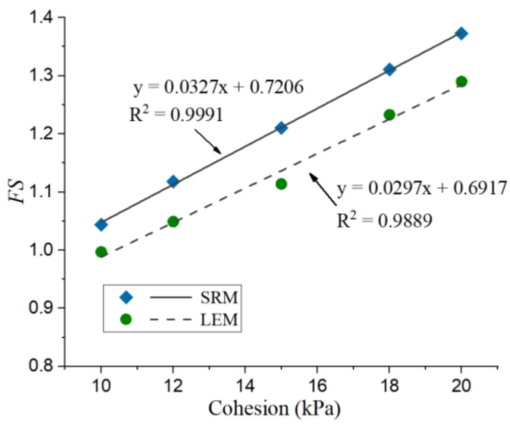

Fig. 7 Relationship between the slope soil cohesion and the *FS*

parameters are illustrated in Fig. 4. As the slope ratio increases, the value of the two strain parameters becomes larger (Fig. 4). This tendency agrees well with the results of a previous experimental study (Keskin and Laman 2013).

Fig. 5 shows the relationship among the ultimate bearing capacity, the average of maximum strains and the *FS*. According to the conventional slope stability analysis theories, the slope ratio can influence the sliding force directly (Abramson *et al.* 2002, Duncan *et al.* 2014). Based on the strain, the *FS* and the ultimate bearing capacity can be estimated. When the slope ratio increases, both the *FS* and the ultimate bearing capacity grow accordingly. The phenomenon can be reflected by the increase of the strain parameter. Besides, similar to the average of maximum strain, the maximum strain also has such a tendency. These phenomena reflect that the two strain parameters can illustrate the slope stability in different ways.

3.2 Influence of soil strength parameters

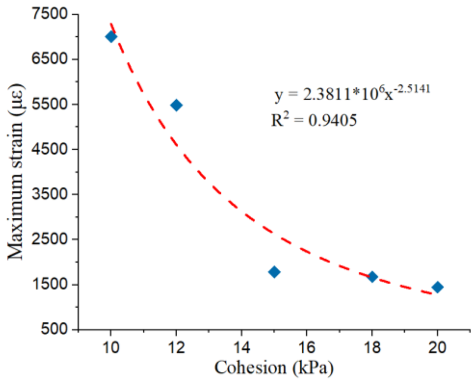

(a) Maximum strain encountered by all the five monitoring lines

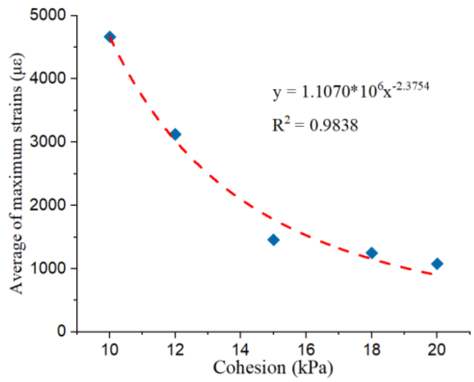

(b) Average of maximum strains encountered by all the five monitoring lines

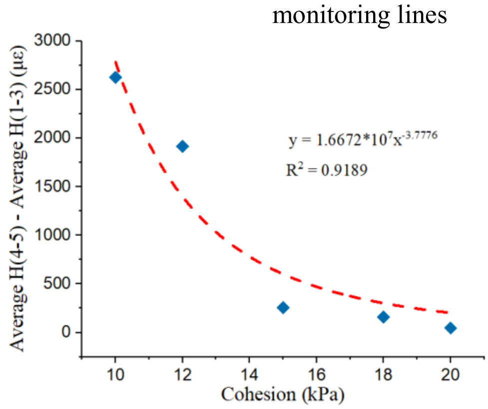

(c) Average of the maximum strain of the No.4 and No.5 monitoring lines subtracting the average of the maximum strain of the No.1 to 3 monitoring lines

Fig. 8 Relationships between the cohesion and strain parameters

3.2.1 Cohesion

Fig. 6 shows the horizontal strain distribution of the slope with different cohesions. For the slope with a lower cohesion, the horizontal strain is larger. Meanwhile, in this condition, a "y" shaped region of large tensile strain emerges, in which the slope failure probably occurs (Zhu *et al.* 2016). In comparison, when the cohesion is high, the large tensile strain region is distributed in a wide range. This strain distribution can eliminate the strain concentration, which retards the slip surface forming. In other words, from the perspective of strain, the critical slip surface can be predicted by the large tensile strain region. This phenomenon is more apparent, for a slope with a smaller soil cohesion.

The ordinary method of slices is a classical one of the LEM family. According to its principle, the *FS* can be expressed as

$$FS = \frac{\sum_{i=1}^{n}\left(c_i l_i + W_i \cos\alpha_i \tan\phi_i\right)}{\sum_{i=1}^{n} W_i \sin\alpha_i} \tag{1}$$

where the subscript i means the block number, c_i and ϕ_i are the soil cohesion and the friction angle of the block, respectively, l_i is the length of the block base, W_i is the weight of the i-th block, and α_i is the inclination angle of the potential failure surface of each slice. According to the simulation setup, the slope is homogenous, so Eq. (1) can be transformed to

$$FS = ac + b\tan\phi \tag{2}$$

where $a = \frac{\sum_{i=1}^{n}(l_i)}{\sum_{i=1}^{n} W_i \sin\alpha_i}$ and $b = \sum_{i=1}^{n}\cot(\alpha_i)$, c and ϕ are the cohesion and friction angle of soil, respectively. From Eq. (2), the *FS* can be obtained through the various c when other parameters remain constant. It means *FS* alters linearly with the change of c. Fig. 7 shows the *FS* results calculated based on LEM and SRM. The LEM results are generally lower than those of the SRM, which have been verified previously (Lu and Godt 2013).

Figs. 8(a) and 8(b) show the empirical relationships between strain parameters and cohesion. The results show that for the slope with a higher cohesion, all strain parameters become smaller, indicating smaller deformation of the slope mass. A new parameter "*D*" is defined as the average of the maximum strains of No. 4 and No. 5 monitoring lines subtracting the average of the maximum strain of No. 1 to 3 monitoring lines . It is used to represent the approximate deformation region of the slope. When the soil cohesion is higher than a certain value, *D* reduces from 2200 με to 250 με and maintains at a low level. This phenomenon indicates that the deformation pattern of the slope transforms from strain concentration to global deformation. To further investigate the deformation

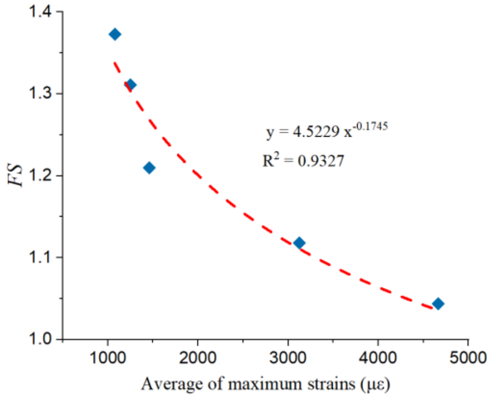

Fig. 9 Relationship between the average of maximum strains encountered by all the five monitoring lines and the *FS*

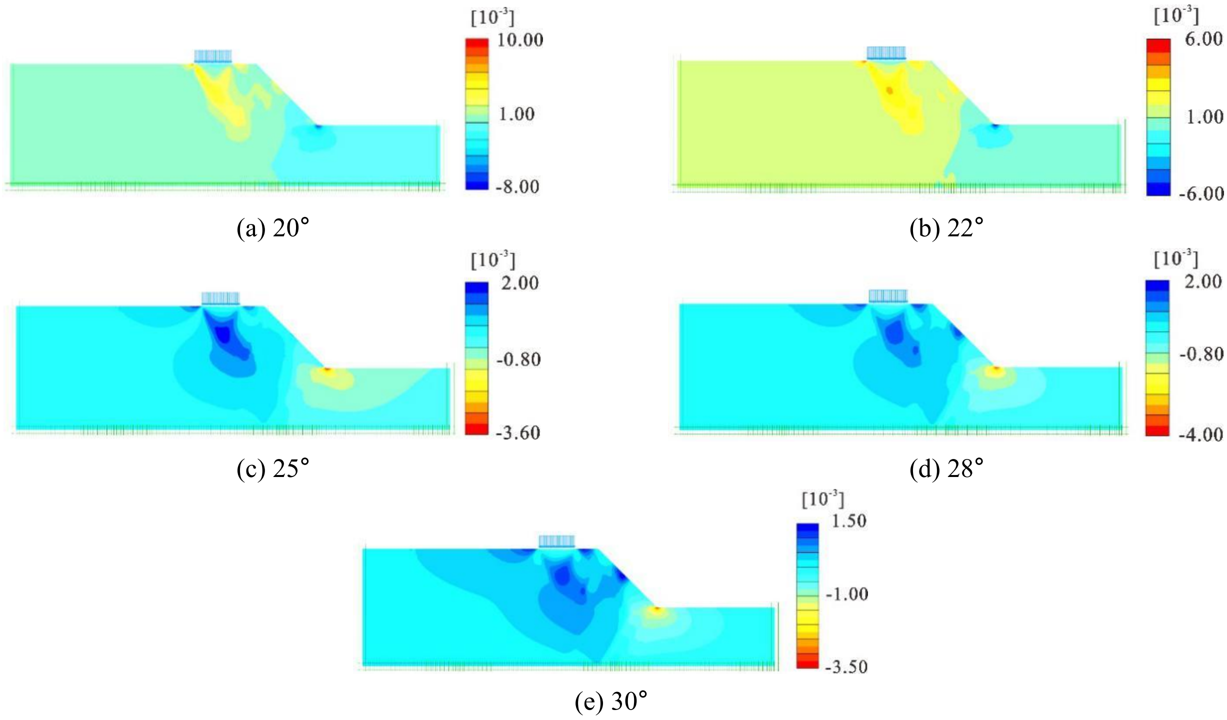

Fig. 10 Contour of the horizontal strain in the slopes with different friction angles

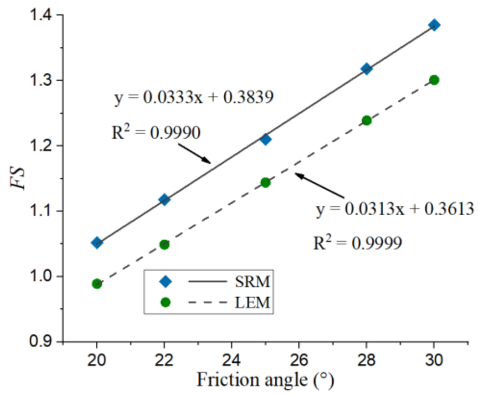

Fig. 11 Relationship between the friction angle and the *FS*

pattern, the exponential function is found to provide the best fit for the relationship between the average of maximum strains and the *FS* (Fig. 9). The relationship verifies the hypothesis that the *FS* will drop with the increase of the average of maximum strains.

3.2.2 Friction angles

Fig. 10 shows the contours of the horizontal strain in the

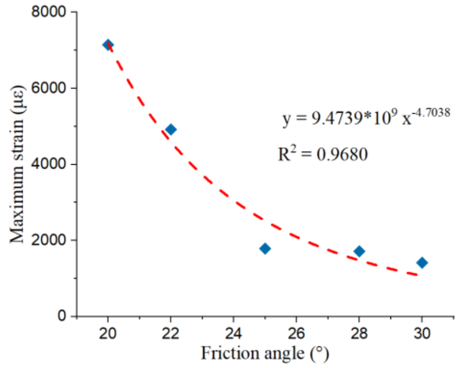

(a) Maximum strain encountered by all the five monitoring lines

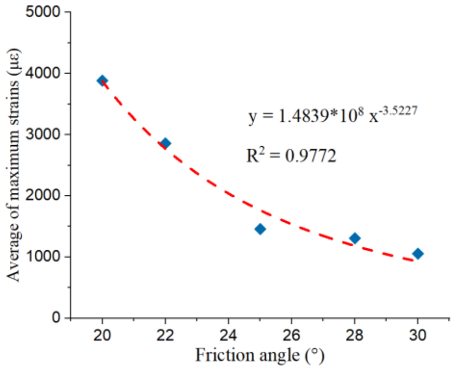

(b) Average of maximum strains encountered by all the five monitoring lines

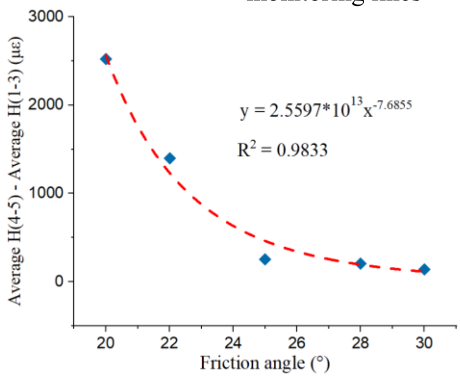

(c) Average of the maximum strain of the No.4 and No.5 monitoring lines subtracting the average of the maximum strain of the No.1 to 3 monitoring lines

Fig. 12 Relationships between the friction angle and strain parameters

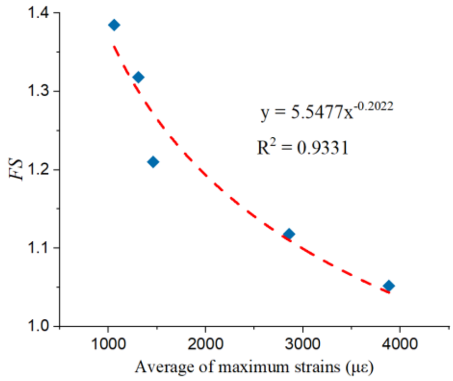

Fig. 13 Relationship between the average of maximum strains encountered by all the five monitoring lines and the *FS*

slopes with various friction angles. The effecting law of friction angle on slope stability is similar to that of cohesion. As the friction angle increases, the horizontal strain becomes smaller. Also, the large tensile strain region gradually expands and the maximum strain slumps accordingly (Fig. 10). From Fig. 10(a) to Fig. 10(c), the large tensile strain region is apparent, and the shape of the region also like a reversed "y". When the friction angle is over 25° (Fig. 10(d) and Fig. 10(e)), the large tensile strain region expands to the large region, which eliminates maximum strain.

Fig. 11 depicts linear relationships between the friction angle and the *FS*. Figs. 12(a) and 12(b) show that the strain parameters have exponential relationships with the friction angle. Both of these strain parameters manifest that the larger friction angle correlates with the lower slope deformation. As shown in Fig. 12(c), when the friction angle is over the value around 22°, the *D* drops dramatically from almost 2500 με to 200 με. Later, for the slope with the larger friction angle, the *D* stays in the low-level value. The phenomenon relates to the changes of slope deformation patterns, which transforms from the strain concentration to the global deformation. These results are similar to the relationships between strain parameters and soil cohesion. Fig. 13 shows the *FS* declines with increase of the average of maximum strains.

Generally, when the slope soil has higher strength, the slope deformation becomes lower accordingly. At the same time, the large tensile strain region expands, and the slope

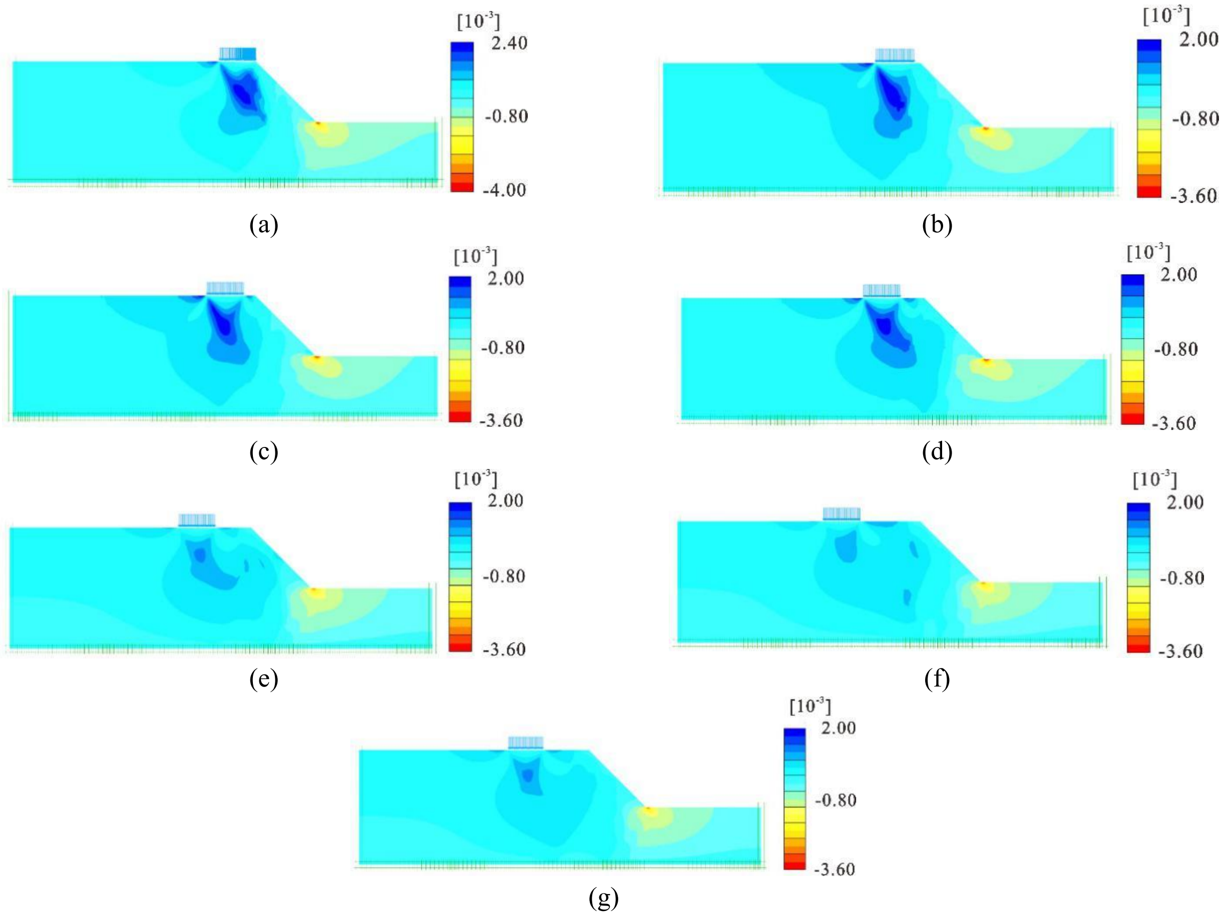

Fig. 14 Contour of horizontal strain in different slopes with different loading locations (a) p = 0 m, (b) p = 1 m, (c) p = 2 m, (d) p = 4 m, (e) p = 6 m, (f) p = 8 m and (g) p = 10 m

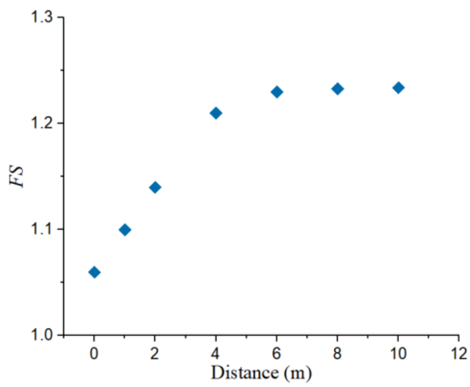

Fig. 15 Relationship between the distance from the slope edge and the *FS*

stability increases. Hence, considering the results of the simulation test, horizontal strain monitoring lines in slopes can be seen as a flexible way to evaluate the slope stability in different soil strength conditions in the field.

3.3 Loading positions

Figs. 14(a)-14(d) shows the large tensile strain region is arc-shaped, which indicates a potential slip surface. As the distance increases, the horizontal strain reduces gradually. Later on, after the distance surpasses 6 m, the strain decreases and the soil deformation becomes lower (Figs.14(e)-14(g)). The shape of the large tensile strain region resembles that of loading on the flat ground.

Fig. 15 displays the variation of slope stability with the change of the distance. The *FS* rises significantly with the increase of the distance (especially within the first 4 m). When the distance is beyond 4 m, the *FS* gradually becomes stable at 1.23. As shown in Fig. 16(a), the average of maximum strains reduces with the growth of the distance. To illustrate the issue specifically, two different stages can be noticed on the full scale from Fig. 16(b) and 16(c). In the first half, the average maximum strains reduce quickly, and then it drops mildly when the distance is beyond 1 m. As

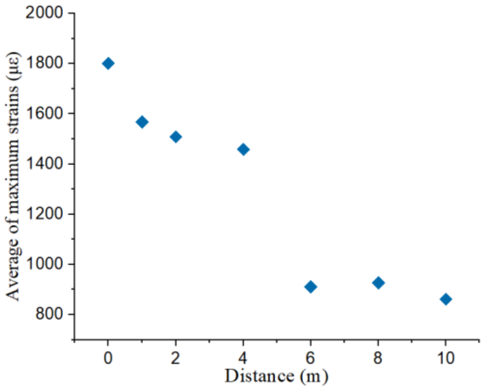

(a) Relationship in the full scale

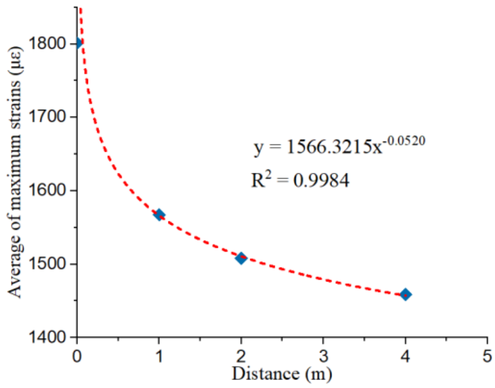

(b) Relationship in the first half scale

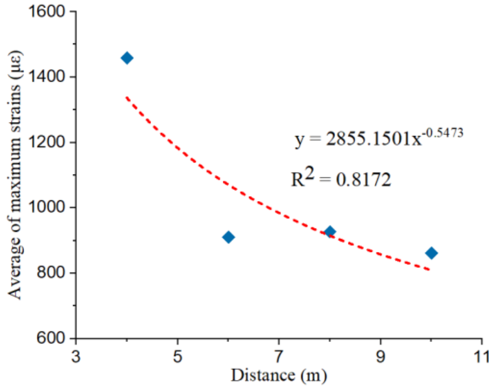

(c) Relationship in the second half scale

Fig. 16 Relationships between the distance and the average of maximum strains encountered by all the five monitoring lines

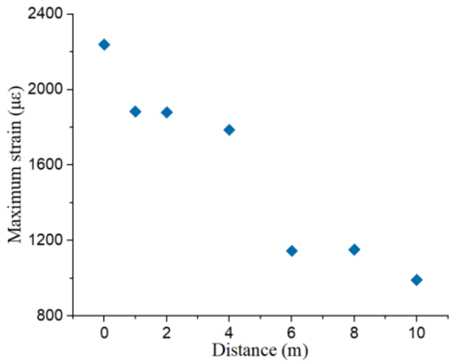

Fig. 17 Relationship between the distance and the maximum strain

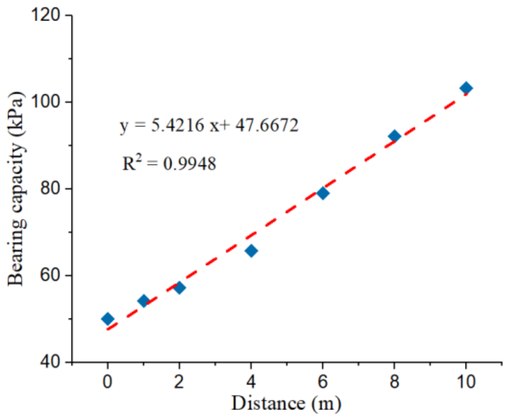

Fig. 18 Relationship between the distance and the ultimate bearing capacity

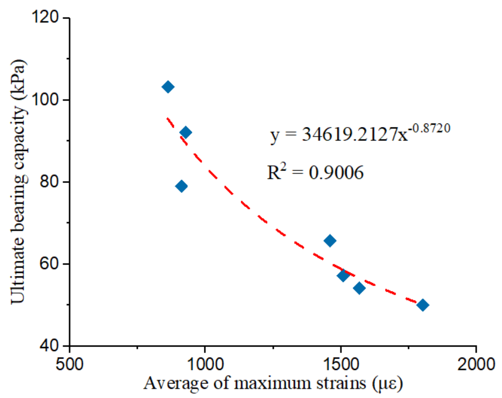

Fig. 19 Relationship between the average of maximum strains encountered by all the five monitoring lines and the ultimate bearing capacity

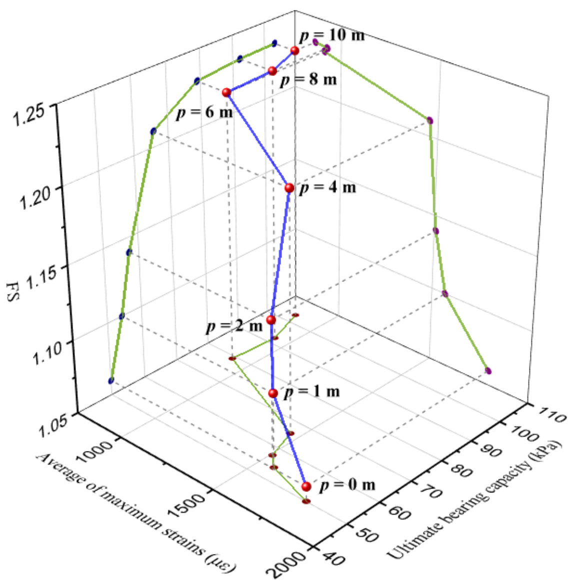

Fig. 20 Relationship between the ultimate bearing capacity, the average of maximum strains encountered by all the five monitoring lines and the *FS*

the distance increases from 4 m to 6 m, the average of maximum strains suddenly diminishes substantially from 1460 με to 920 με. This phenomenon can be illustrated by that the loading gradually deviates from the critical stability zone of the slope. After the distance surpasses 6 m, the average of maximum strains becomes stable. Fig. 17 reveals the similar relationship between the distance and the maximum strain, which can be interpreted in a similar way as above.

Based on the DLO method, the ultimate bearing capacity is figured out. The relationship between the distance and the ultimate bearing capacity is presented in Fig. 18. The ultimate bearing capacity grows with the increase of the distance, but this is true only within a certain range. When the distance exceeds a proper range, the increase of the ultimate bearing capacity will slow down and the ultimate bearing capacity will gradually become stable (Pantelidis and Griffiths 2015). As shown in Fig. 19, the relationship between the average of maximum strains and the ultimate bearing capacity can be fitted by an exponential function. The strain parameter can be used to estimate the ultimate bearing capacity of the slope in this situation.

The relationships between the ultimate bearing capacity, the average of maximum strains and the *FS* are shown in Fig. 20. Unlike the relationship between the distance and the ultimate bearing capacity, the variation of the *FS* exhibits different characteristics. At first, the *FS* climbs when the distance increases near the slope edge. Later, the *FS* gradually becomes stable despite of the increase of the distance. In other words, the ultimate bearing capacity in the loading position can hardly influence the *FS* of the slope when the distance is over 4 m. Compared with estimating the ultimate bearing capacity, the strain can reflect the slope stability more effectively. The gradual decrease of the strain parameter can illustrate an increasing tendency of the *FS* when the distance is within 4 m. When the distance is over 4 m, the strain parameter keeps almost constant. This phenomenon illustrates that the slope deformation does not expand, which corresponds well with the negligible change of the *FS*. The results in Fig. 20 show that the strain parameter can be used to evaluate slope stability properly. Generally, the increases of strain parameters are related to the variation of slope stability and ultimate bearing capacity. In fieldwork, when strain sensors are applied, the strain measured and its changing characteristic should be correlated with slope stability and ultimate bearing capacity, which can be employed to estimate the geoenvironmental safety in a region.

4. Conclusions

In this paper, the feasibility of strain-based slope stability analysis has been evaluated under different slope conditions. The conclusions drawn in this study are as follows:

- Slope ratio can significantly influence slope stability. The strain parameters can properly reflect the influence of the slope ratio. In the general trend, the strain parameters reduce with the decrease of the slope ratio. The relationships between strain parameters and *FS* can be fitted well by using exponential functions.
- The *FS* has a positive correlation with the soil strength parameters. The change of the cohesion and the change of friction angle have well exponential relationships with the change of the average maximum strain correspondingly. Such relationships can be used to estimate slope stability from the strain. For the slope with higher soil cohesion, the strain concentration becomes lower accordingly. A similar phenomenon occurs in the model with the various friction angles.
- Slope strain parameters decrease with the increase of the distance from the slope edge. When the loading is near the slope edge, strain parameters reduce apparently with the growth of the distance. After the loading exceeds the critical stability zone, strain parameters decrease dramatically to the lower state and the ultimate bearing capacity enhanced accordingly. In this situation, the shape of the large tensile

strain region is like that of loading on the flat ground. The changing characteristic of the *FS* corresponds well with strain parameters.

The strain analysis is reasonable for estimating slope stability in different conditions. Such findings shed critical light on establishing a high-precision slope monitoring system based on distributed fiber optic sensing (DFOS). However, slope stability may be influenced by weak intercalated layers, reinforcing elements, rainfall infiltration, and other environmental factors, which are not included in the study. These factors may influence the deformation characteristics of slopes, which needs to be further studied.

Acknowledgments

The authors gratefully acknowledge the financial support provided by the National Natural Science Foundation of China (No. 41722209, 42077235), the National Key Research and Development Program of China (No. 2018YFC1505104), and the Open Fund of Key Laboratory of Mountain Hazards and Earth Surface Processes, Chinese Academy of Sciences.

References

Abramson, L.W., Lee, T.S., Sharma, S. and Boyce, G.M. (2002), *Slope Stability and Stabilization Methods*, John Wiley & Sons, Hoboken, New Jersey, U.S.A.

Aminpour, M.M., Maleki, M. and Ghanbari, A. (2017), "Investigation of the effect of surcharge on behavior of soil slopes", *Geomech. Eng.*, **13**(4), 653-669. https://doi.org/10.12989/gae.2017.13.4.653.

Angeli, M.G., Pasuto, A. and Silvano, S. (2000), "A critical review of landslide monitoring experiences", *Eng. Geol.*, **55**(3), 133-147. https://doi.org/10.1016/S0013-7952(99)00122-2.

Cheng, Y.M., Lansivaara, T. and Wei, W.B. (2007), "Two-dimensional slope stability analysis by limit equilibrium and strength reduction methods", *Comput. Geotech.*, **34**(3), 137-150. https://doi.org/10.1016/j.compgeo.2006.10.011.

Das, B.M. (2015), *Principles of Foundation Engineering*, Cengage Learning, Connecticut, U.S.A.

Duncan, J.M., Wright, S.G. and Brandon, T.L. (2014), *Soil Strength and Slope Stability*, John Wiley & Sons, Virginia, U.S.A.

El Sawwaf, M. (2010), "Experimental and numerical study of strip footing supported on stabilized sand slope", *Geotech. Geol. Eng.*, **28**(4), 311-323. https://doi.org/10.1007/s10706-009-9293-9.

Florkiewicz, A. and Kubzdela, A. (2013), "Factor of safety in limit analysis of slopes", *Geomech. Eng.*, **5**(5), 485-497. https://doi.org/10.12989/gae.2013.5.5.485.

Georgiadis, K. (2009), "Undrained bearing capacity of strip footings on slopes", *J. Geotech. Geoenviron. Eng.*, **136**(5), 677-685. https://doi.org/10.1061/(ASCE)GT.1943-5606.0000269.

Griffiths, D.V. and Lane, P.A. (1999), "Slope stability analysis by finite elements", *Geotechnique*, **49**(3), 387-403. https://doi.org/10.1680/geot.1999.49.3.387.

Humpheson, C. and Lewis, R. (1975), "Associated and non-associated visco-plasticity in soils mechanics", *Geotechnique*, **25**(5), 671-689. https://doi.org/10.1680/geot.1975.25.4.671.

Keskin, M.S. and Laman, M. (2013), "Model studies of bearing capacity of strip footing on sand slope", *KSCE J. Civ. Eng.*, **17**(4), 699-711. https://doi.org/10.1007/s12205-013-0406-x.

Leshchinsky, B. (2014), "Limit analysis optimization of design factors for mechanically stabilized earth wall-supported footings", *Transport. Infrastruct. Geotechnol.*, **1**(2), 111-128. https://doi.org/10.1007/s40515-014-0005-4.

Leshchinsky, B. (2015), "Bearing capacity of footings placed adjacent to c′-ϕ′ slopes", *J. Geotech. Geoenviron. Eng.*, **141**(6), 04015022. https://doi.org/10.1061/(ASCE)GT.1943-5606.0001306.

Li, H.J., Zhu, H.H., Li, Y.H., Hu, W. and Shi, B. (2020), "Fiber Bragg grating-based flume test to study the initiation of landslide-debris flows induced by concentrated runoff", *Geotech. Test. J.*, **44**. In Press. https://doi.org/10.1520/GTJ20190290.

Liu, D. and Chen, X. (2015), "Shearing characteristics of slip zone soils and strain localization analysis of a landslide", *Geomech. Eng.*, **8**(1), 33-52. https://doi.org/10.12989/gae.2015.8.1.033.

Liu, Z., Su, L., Zhang, C., Iqbal, J. Hu, B. and Dong, Z. (2020), "Investigation of the dynamic process of the xinmo landslide using the discrete element method", *Comput. Geotech.*, **123**, 103561. https://doi.org/10.1016/j.compgeo.2020.103561.

Lu, N. and Godt, J.W. (2013), *Hillslope Hydrology and Stability*, Cambridge University Press, Cambridge, U.K.

McCombie, P.F. (2009), "Displacement based multiple wedge slope stability analysis", *Comput. Geotech.*, **36**(1-2), 332-341. https://doi.org/10.1016/j.compgeo.2008.02.008.

Ouch, R., Ukritchon, B., Pipatpongsa, T. and Khosravi, M.H. (2017), "Finite element analyses of the stability of a soil block reinforced by shear pins", *Geomech. Eng.*, **12**(6), 1021-1046. https://doi.org/10.12989/gae.2017.12.6.1021.

Pantelidis, L. and Griffiths, D.V. (2015), "Footing on the crest of slope: Slope stability or bearing capacity?", *Eng. Geol. Soc. Territory*, **2**, 1231-1234. H ttps://doi.org/10.1007/978-3-319-09057-3_215.

Pei, H., Zhang, S., Borana, L., Zhao, Y. and Yin, J. (2019), "Slope stability analysis based on real-time displacement measurements", *Measurement*, **131**, 686-693. https://doi.org/10.1016/j.measurement.2018.09.019.

Plaxis (2002), *User Manual, 2D Version8*. Delft University of Technology & PLAXIS b.v., Delft, The Netherlands

Sasahara, K. (2017), "Prediction of the shear deformation of a sandy model slope generated by rainfall based on the monitoring of the shear strain and the pore pressure in the slope", *Eng. Geol.*, **224**, 75-86. https://doi.org/10.1016/j.enggeo.2017.05.003.

Severin, J., Eberhardt, E., Leoni, L. and Fortin, S. (2014), "Development and application of a pseudo-3D pit slope displacement map derived from ground-based radar", *Eng. Geol.*, **181**, 202-211. https://doi.org/10.1016/j.enggeo.2014.07.016.

Smith, C. and Gilbert, M. (2007), "Application of discontinuity layout optimization to plane plasticity problems", *Proc. Royal Soc. A Math. Phys. Eng. Sci.*, **463**(2086), 2461-2484. https://doi.org/10.1098/rspa.2006.1788.

Song, Z., Shi, B., Juang, H., Shen, M. and Zhu, H. (2017), "Soil strain-field and stability analysis of cut slope based on optical fiber measurement", *B. Eng. Geol. Environ.*, **76**(3), 937-946. https://doi.org/10.1007/s10064-016-0904-4.

Su, L.J., Xu, X.Q., Geng, X.Y. and Liang, S.Q. (2017), "An integrated geophysical approach for investigating hydro-geological characteristics of a debris landslide in the Wenchuan Earthquake Area", *Eng. Geol.*, **219**, 52-63. https://doi.org/10.1016/j.enggeo.2016.11.020.

Sun, Y.J., Zhang, D., Shi, B., Tong, H.J., Wei, G.Q. and Wang, X. (2014), "Distributed acquisition, characterization and process analysis of multi-field information in slopes", *Eng. Geol.*, **182**,

49-62. https://doi.org/10.1016/j.enggeo.2014.08.025.
Tu, Y., Zhong, Z., Luo, W., Liu, X. and Wang, S. (2016), "A modified shear strength reduction finite element method for soil slope under wetting-drying cycles", *Geomech. Eng.*, **11**(6), 739-756. https://doi.org/10.12989/gae.2016.11.6.739.
Uchimura, T., Towhata, I., Anh, T.T.L., Fukuda, J., Bautista, C.J., Wang, L, Seko, I., Uchida, T., Matsuoka, A., Ito, Y., Onda, Y., Iwagami, S., Kim, M. and Sakai, N. (2010), "Simple monitoring method for precaution of landslides watching tilting and water contents on slopes surface", *Landslides*, **7**(3), 351-357. https://doi.org/10.1007/s10346-009-0178-z.
Xing, H., Liu, L. and Luo, Y. (2019), "Water-induced changes in mechanical parameters of soil-rockmixture and their effect on talus slope stability", *Geomech. Eng.*, **18**(4), 353-362. https://doi.org/10.12989/gae.2019.18.4.353.
Yang, G., Zhong, Z., Zhang, Y. and Fu, X. (2015), "Optimal design of anchor cables for slope reinforcement based on stress and displacement fields", *J. Rock Mech. Geotech. Eng.*, **7**(4), 411-420. https://doi.org/10.1016/j.jrmge.2015.04.004.
Yang, X.L., Wang, Z.B., Zou, J.F. and Li, L. (2007), "Bearing capacity of foundation on slope determined by energy dissipation method and model experiments", *J. Cent. South Univ. T.*, **14**(1), 125-128. https://doi.org/10.1007/s11771-007-0025-0.
Zhang, C.C., Zhu, H.H., Liu, S.P., Shi, B. and Zhang, D. (2018), "A kinematic method for calculating shear displacements of landslides using distributed fiber optic strain measurements", *Eng. Geol.*, **234**, 83-96. https://doi.org/10.1016/j.enggeo.2018.01.002.
Zhu, H.H., Shi, B., Yan, J.F., Zhang, J., Zhang, C.C. and Wang, B.J. (2014), "Fiber Bragg grating-based performance monitoring of a slope model subjected to seepage", *Smart Mater. Struct.*, **23**(9), 1-12. https://doi.org/10.1088/0964-1726/23/9/095027.
Zhu, H.H., Wang, Z.Y., Shi, B. and Wong, J.K.W. (2016), "Feasibility study of strain based stability evaluation of locally loaded slopes: Insights from physical and numerical modeling", *Eng. Geol.*, **208**, 39-50. https://doi.org/10.1016/j.enggeo.2016.04.019.
Zienkiewicz, O.C., Humpheson, C. and Lewis, R.W. (1975), "Associated and non-associated visco-plasticity and plasticity in soil mechanics", *Geotechnique*, **25**(4), 671-689. https://doi.org/10.1680/geot.1975.25.4.671.

CC